iScience

Article

Porous CeO_2 nanozyme with visible-light-enhanced catalase-mimicking activities by ligand-to-metal charge transfer

Graphical abstract

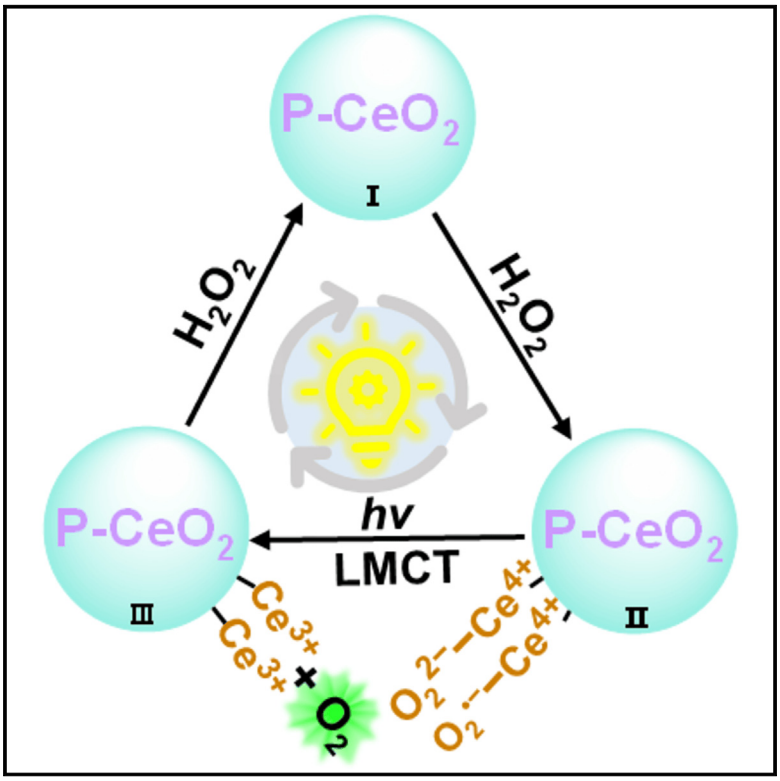

Highlights

- P-CeO_2 exhibits a 2-fold increase in catalase-like activity under visible light
- Discovery of a ligand-to-metal charge transfer (LMCT) band on P-CeO_2 via peroxide adsorption
- Unveiling the mechanism of visible-light-enhanced catalase-like activity in P-CeO_2

Authors

Pengju Li, Wei Yuan, Ke Hu

Correspondence

yuanwei@fudan.edu.cn (W.Y.),
khu@fudan.edu.cn (K.H.)

In brief

Catalysis; Nanoparticles; Biocatalysis; Nanomaterials

Li et al., 2025, iScience *28*, 112149
April 18, 2025
https://doi.org/10.1016/j.isci.2025.112149

CellPress

iScience

CellPress
OPEN ACCESS

Article

Porous CeO_2 nanozyme with visible-light-enhanced catalase-mimicking activities by ligand-to-metal charge transfer

Pengju Li,[1] Wei Yuan,[2,*] and Ke Hu[1,3,*]

[1]Department of Chemistry and Shanghai Key Laboratory of Molecular Catalysis and Innovative Materials, Fudan University, Shanghai 200438, China

[2]Shanghai Frontiers Science Research Base of Intelligent Optoelectronics and Perception, Institute of Optoelectronics, Fudan University, Shanghai 200438, China

[3]Lead contact

*Correspondence: yuanwei@fudan.edu.cn (W.Y.), khu@fudan.edu.cn (K.H.)

https://doi.org/10.1016/j.isci.2025.112149

SUMMARY

Nanozymes are promising synthetic alternatives to natural enzymes owing to their unique physical and chemical properties, but improving their thermocatalytic activity often involves complex procedures. This study introduces a light-induced approach to enhance the catalytic activity of facilely prepared porous cerium oxide (P − CeO_2) nanozymes. Under visible light irradiation, the catalytic efficiency (k_{cat}/K_m) of the P − CeO_2 more than doubles compared to its thermocatalytic efficiency. Spectroscopic analyses reveal that this enhancement stems from a ligand-to-metal charge transfer (LMCT) band, arising from peroxide species adsorbed on the P − CeO_2 surface. As a practical demonstration, P-CeO2 exhibits visible-light enhanced scavenging of reactive oxygen species (ROS) *in vitro*. Overall, this study provides new mechanistic insights of using LMCT-induced visible light catalysis for the improvement of catalytic activity of light-responsive nanozymes.

INTRODUCTION

Nanozymes, as artificial nano-structured biomimetic enzymes, have unique physicochemical and biocatalytic characteristics as well as tunable catalytic activities. Nanozymes have been widely used in biomedical sensing,[1,2] antimicrobial,[3,4] tumor therapy,[5,6] and other biological fields.[7–10] In order to better replace the natural enzymes, the effective improvement of the catalytic activity of nanozymes has become one of the prerequisites for its development. Currently, great efforts have been made to improve their thermocatalytic activity, including adjusting their sizes,[11] compositions,[12] morphology,[13] and crystal facets (Figure 1A).[14] However, these nanomaterial engineering require laborious procedures and delicate synthetic conditions, which may be hard to replicate and thereby limit future practical applications. Therefore, it is important to develop simple methods to accurately regulate the catalytic activity of nanozymes.

In the natural photosystems, photo-biocatalytic conversion can be accomplished by light-induced multi-electron and proton transfer.[15–17] In addition, light is widely used in semi-artificial photosynthesis systems as a source of renewable energy and environmentally friendly synthetic reagent.[18–20] Nanoparticles can absorb photons and be in an excited state, generating high-energy electrons or holes for various chemical reactions and biocatalytic reactions.[21–24] Moreover, the rate of catalytic reaction can be controlled precisely by adjusting the wavelength and intensity of the incident light.[25–27] At the same time, most of the nanozymes belong to oxidoreductases, which use the active central sites of redox metal ion pairs to exchange electrons to catalyze the redox transformation of substrates, so as to realize the enzyme-like catalytic activity of the nanozymes.[28–30] Therefore, improving the catalytic activity of nanozymes through photo-induced charge transfer shows a broad prospect in the light-responsive nanozyme systems.

Nanomaterials with redox active sites are very important in catalytic reaction applications.[31,32] Cerium oxide nanoparticles (CeO_2 NPs) have attracted widespread attention in catalysis and antioxidant treatment of reactive oxygen species (ROS)-related diseases due to the excellent physicochemical properties that can be cycled between Ce^{3+} and Ce^{4+}[33,34]. The Ce^{4+}/Ce^{3+} redox pair on the surface of cerium oxide can decompose H_2O_2 to generate H_2O and O_2, showing the characteristics of catalase-like nanozymes.[35,36] However, it is very challenging to further improve the catalase-like catalytic activity of CeO_2 by controlling its composition and crystal faces.

Herein, we successfully used a simple synthetic procedure to construct a nanozyme (porous CeO_2 NPs, P − CeO_2) that has visible-light-enhanced catalase-mimicking activities (Figure 1B). The enhanced activities were found to be attributed to the excitation of a previously unknown ligand-to-metal charge transfer

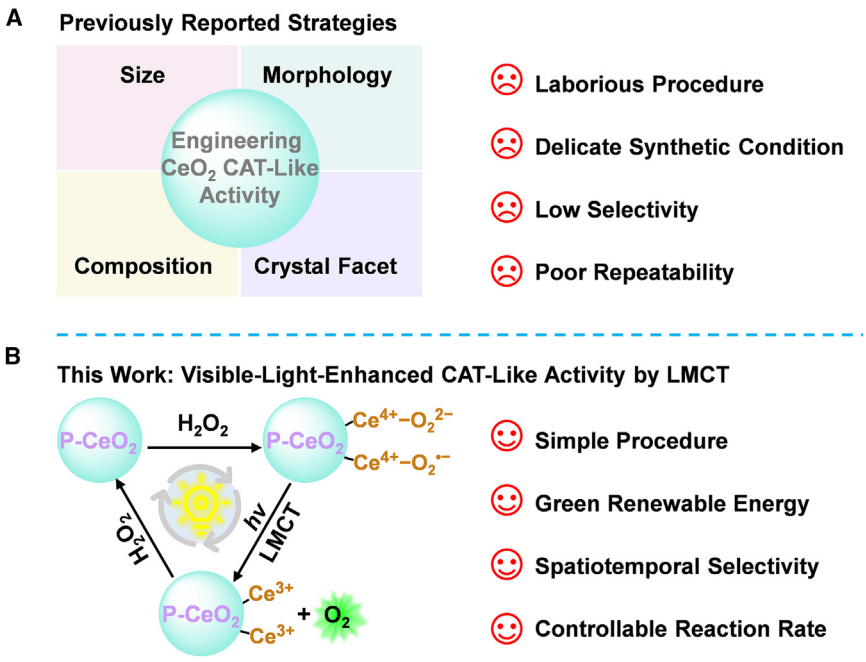

Figure 1. Strategies for improving the catalytic activity of CeO_2 catalase-like

(LMTC) band induced by the adsorption of hydrogen peroxide to P – CeO_2. Light-induced LMCT can accelerate the release of O_2 from the thermodynamically stable Ce – O_2^- – / O_2^- – / complex on the surface of P – CeO_2. The process of charge transfer and material transformation during the photo-induced reaction between P – CeO_2 and substrate H_2O_2 was revealed by a combination of spectroscopic techniques including transient absorption (TA) spectroscopy, electron spin resonance (ESR), X-ray photoelectron spectroscopy (XPS), and Fourier transform infrared (FT-IR) spectra. Moreover, the results of enzyme kinetic parameters showed that the catalytic efficiency of P – CeO_2 nanozyme is increased by 105% and 123% under 405 nm and 450 nm laser irradiation, respectively. And the O_2 production rate was light wavelength and power dependent. The visible-light-enhanced catalase-like activity of P – CeO_2 was also confirmed at the cellular level. We believe that this study will not only help to understand the catalytic mechanism of P – CeO_2 catalase-like nanozymes, but also promote the extensive exploration of light-responsive nanozymes.

RESULTS AND DISCUSSION

Synthesis and characterization of P – CeO_2 NPs

P – CeO_2 NPs were fabricated by using a facile one-step strategy, according to the reported method with slight modification.[37] Transmission electron microscopy (TEM) and high-resolution transmission electron microscope (HR-TEM) images indicated that the as-synthesized P – CeO_2 NPs were assembled from nano-crystalline particles with a uniform spherical morphology and an average diameter of approximately 50 nm (Figures 2A, 2B, and S1). Dynamic light scattering (DLS) measurement demonstrated that P – CeO_2 NPs in solution possessed narrow size distribution with an average hydrodynamic diameter of about 85 nm (Figure 2C). The element mapping images exhibited that the Ce and O elements are evenly distributed throughout the P – CeO_2 NPs (Figure 2D). Furthermore, the energy dispersive X-ray spectroscopy (EDX) also confirmed the composition of Ce and O elements, demonstrating the successful synthesis of P – CeO_2 NPs (Figure S2). The crystal fine structure of the P – CeO_2 NPs was further elucidated by powder X-ray diffraction (XRD, Figure 2E). XRD pattern clearly revealed that P – CeO_2 NPs presented the characteristic diffraction peaks of cubic phase (JCPDS No. 34-0349). Consistently, high resolution transmission electron microscope (HRTEM) image presented the lattice fringe with an inter-planar spacing of 0.31 nm (Figure 2B, inset image), which well corresponded to the (111) plane of P – CeO_2 NPs.

The N_2 adsorption/desorption isotherms and pore size distribution plots of P – CeO_2 NPs were also measured (Figure 2F). The data elucidated that surface area and pore size of P – CeO_2 NPs are 180 m^2g^{-1} and 3.4 nm, respectively. In addition, The UV-vis absorption spectrum showed the broad absorption of P – CeO_2 NPs from the near-ultraviolet to the visible region (Figure 2G). This broadened absorption may be caused by different levels of defect states on the surface of the P – CeO_2 NPs, such as oxygen vacancies or Ce^{3+}.

Characterization of light-enhanced catalase-mimicking activities of P – CeO_2 nanozyme

To systematically evaluate whether P – CeO_2 has catalase-like activity that decomposes H_2O_2 to produce O_2 and H_2O, an oxygen sensor was employed to measure O_2 production from light irradiated P – CeO_2 samples. The results showed that P – CeO_2 efficiently catalyzed the decomposition of H_2O_2 in a concentration-dependent manner, and the O_2 production was significantly enhanced as the concentration increases (Figure S3A). At the same time, P – CeO_2 also exhibited moderate potential to decompose H_2O_2 under acidic conditions (Figure S4A). Although P – CeO_2 have shown the catalase-mimicking potential, it is important to further improve its catalytic activity. In nature, many light-related oxidoreductases can achieve photocatalytic biochemical conversion by absorbing photons to induce electron transfer between the enzyme and the substrate.[38–40] Inspired by nature, it is hypothesized that P – CeO_2 can also regulate the catalytic activity of its catalase-like through visible light. Therefore, the improved catalase-like activities of P – CeO_2 were investigated under different

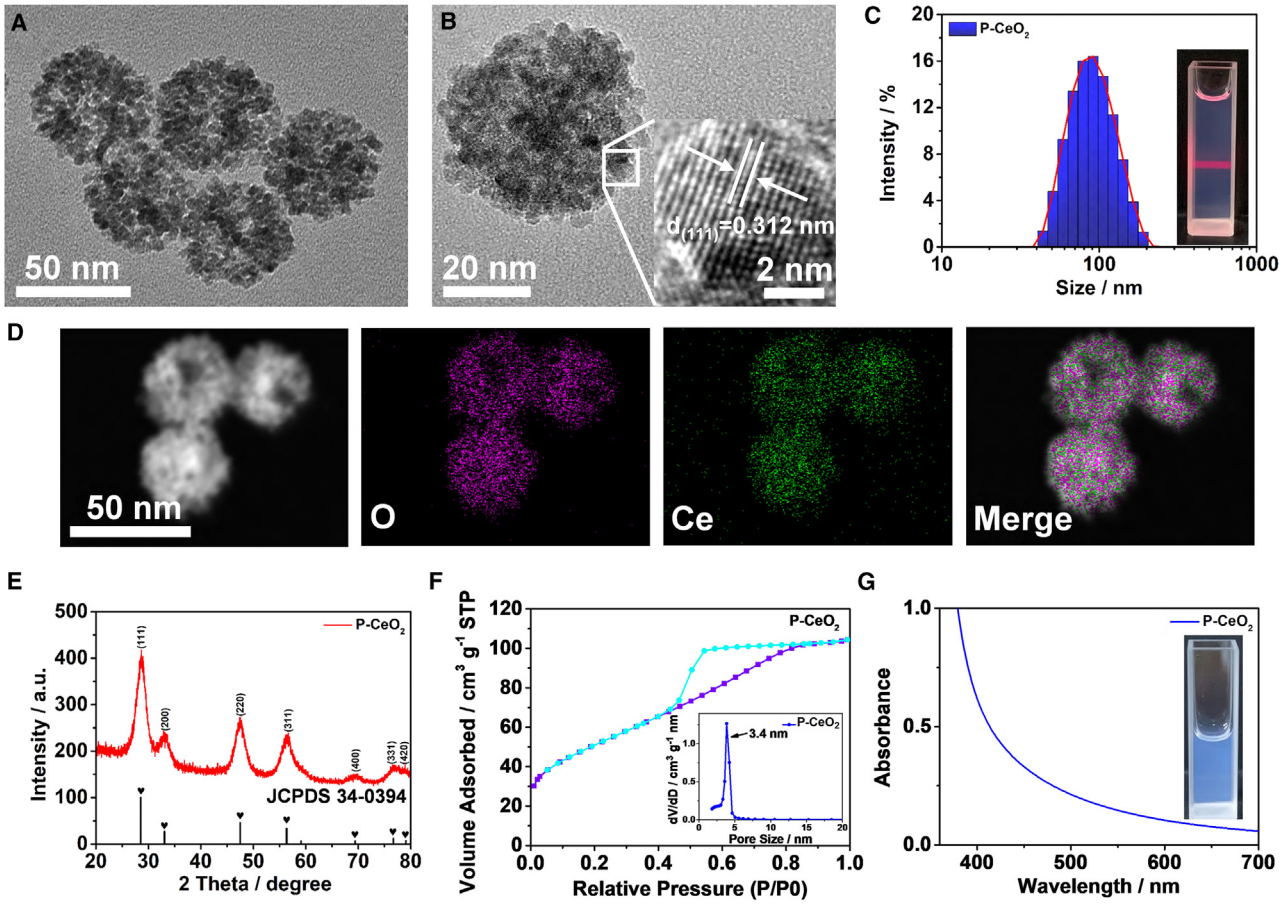

Figure 2. Characterization of P – CeO_2 NPs

(A) TEM images of P – CeO_2 NPs.

(B) HR-TEM image of P – CeO_2 NPs.

(C) Size distribution of P – CeO_2 NPs measured by DLS.

(D) Elemental mapping of P – CeO_2 NPs.

(E) XRD pattern of P – CeO_2 NPs.

(F) Nitrogen adsorption-desorption isotherm of P – CeO_2 NPs. The inset shows the pore size distribution plot of P – CeO_2 NPs.

(G) UV-vis absorption spectrum of P – CeO_2 NPs, where the inset is the photograph of the P – CeO_2 NPs dispersion.

wavelengths of monochromatic laser irradiation. The catalase-like activity of P – CeO_2 was significantly increased by 405 nm or 450 nm laser irradiation than that without irradiation (Figures S3B and S3C). Moreover, P – CeO_2 also showed an obvious light-enhanced catalase-mimicking activities in acidic buffer solution (Figures S4B and S4C), indicating P – CeO_2 NPs could have the potential to accelerate the decomposition of H_2O_2 through light irradiation under acidic microenvironment that often appears in tumorous cells, thereby reducing the level of ROS. In addition, compared with natural catalase, P – CeO_2 also maintained higher catalytic activity in a wide pH range (Figures S5 and S6A). Next, we investigated whether the catalytic active sites can be controlled by turning the laser on and off. First, when P – CeO_2 buffer solution was incubated with H_2O_2, the O_2 concentration in the solution was monitored in real time. When the reaction reached 120 s, the O_2 concentration exhibited a significantly increase under the 405 nm laser irradiation from 120 s to 240 s. In contrast, no obvious increase of O_2 concentration was observed from 240 s to 360 s without laser irradiation (Figure 3A). Similarly, after exposure to 450 nm or 532 nm laser irradiation, the catalase-like activity of P – CeO_2 was significantly enhanced, respectively (Figures 3D and S7).

The catalytic activity of P – CeO_2 NPs toward decomposition of H_2O_2 was evaluated by Michaelis-Menten kinetic assay. According to the initial reaction rates and the corresponding H_2O_2 concentrations, typical Michaelis-Menten saturation curves were obtained by fitting (Figure 3B). To obtain the K_m (Michaelis-Menten constant) and v_{max} (maximum initial velocity), the Lineweaver-Burk and double reciprocal plot of the Michaelis-Menten equation was converted (Equation 1) as shown in Figure 3C. The values of K_m and v_{max} were calculated to be 4.69 mM and 11.7×10^{-7}M s^{-1}, respectively. Simultaneously, catalytic rate constant k_{cat} and catalytic efficiency k_{cat}/K_m were determined to be $1.22\times10^{6}s^{-1}$ and $2.60\times8M^{-1}s^{-1}$ for P – CeO_2 nanozyme. Compared with the natural catalase, the smaller K_m value of P – CeO_2 represents its better affinity with

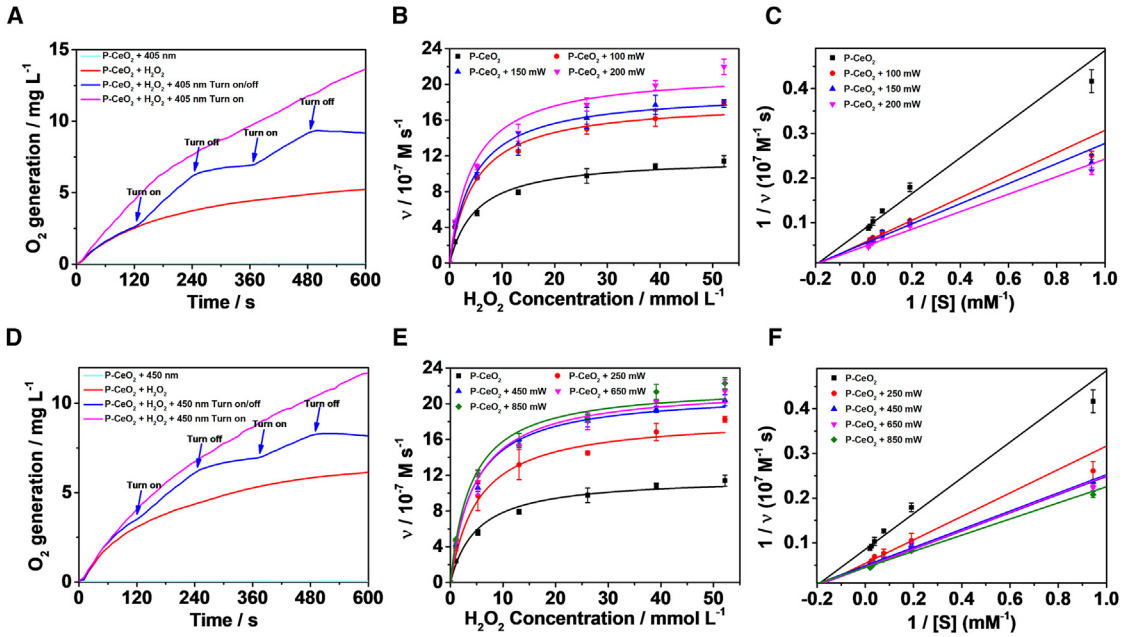

Figure 3. Characterization of light-enhanced catalase-mimicking activities of P – CeO_2 nanozyme

(A and D) Regulation of catalase-like activities of P – CeO_2 under dark, with 405 nm or 450 nm laser irradiation, respectively.

(B and E) Steady-state kinetic assay using the Michaelis-Menten model.

(C and F) Lineweaver-Burk plotting for P – CeO_2 nanozyme under dark, with different 405 nm or 450 nm laser power irradiation, respectively. Turn on (laser on), turn off (laser off).

Data points and error bars are the mean values and standard deviations from three sets of parallel experiments. The initial steady-state catalytic velocities (v) were calculated from the initial slopes of O_2 generation versus time plots in each experiment. All experiments were repeated three times and were performed at room temperature (25°C).

the substrate H_2O_2 (Figures S6B and S6C). Intriguingly, the steady-state kinetics of catalase-like P – CeO_2 is still consistent with the Michaelis-Menten equation model under 405 nm or 450 nm laser irradiation (Figures 3B and 3E). Moreover, light-fluence-dependent data reveals that the reaction rate and catalytic efficiency are significantly dependent on the laser power. Under 405 nm and 450 nm laser irradiation, the catalytic efficiency k_{cat}/K_m of the P – CeO_2 nanozyme is increased by 105% and 123%, respectively (Figures 3C and 3F; Table 1), indicating the enhanced catalase-like activity by visible-light irradiation.

$$\frac{1}{v_0} = \frac{K_m}{v_{max}} \times \frac{1}{[S]} + \frac{1}{v_{max}} \quad \text{(Equation 1)}$$

Analysis of surfaces valence states in P – CeO_2 nanozyme

In particular, CeO_2 NPs are used as effective antioxidants due to the redox changes between Ce^{4+} and Ce^{3+} ions on their surfaces. In general, CeO_2 NPs with a higher percentage of Ce^{4+} showed a more significant catalase-like activity on the decomposition of H_2O_2.[35] To examine the change of Ce element valence states during the reaction, XPS analysis was performed. The high-resolution Ce 3D XPS spectra showed that six of the peaks can be attributed to the Ce^{4+} state (peaks at 882.6, 888.3, 898.2, 901, 907, and 916.4 eV), while the other two are in the Ce^{3+} state (peaks at 885.5 and 904 eV). The results confirmed that the Ce^{4+} state content of the P – CeO_2 was about 78.7% (Figure 4A), which ensured the antioxidant activity being catalase-like. When H_2O_2 was added, the Ce^{4+} state content dropped to 69.6% (Figure 4B). The decrease in the Ce^{4+} state content may be due to the reduction to Ce^{3+} state by H_2O_2 (Equation 2). To explore the reason why visible light enhances the catalase-like activity of P – CeO_2, Ce^{4+} state content under the condition of P – CeO_2 + H_2O_2 + 405 nm was also measured. Intriguingly, after 405 nm laser irradiation, the Ce^{4+} state content recovered to 79.3% (Figure 4C). The results showed that laser irradiation may promote the remodeling of Ce^{4+} active sites and accelerate the forward reaction of Equation 2 to ensure the enhancement of the catalytic activity.

$$H_2O_2 + 2Ce^{4+} \rightarrow 2H^+ + O_2 + 2Ce^{3+} \quad \text{(Equation 2)}$$

To gain a deep insight into the reaction process of P – CeO_2 and H_2O_2, a steady-state UV-vis absorption spectrometer was employed to detect its optical spectral changes in real time. The steady-state spectrum showed that cerium oxide has a strong absorption edge below 500 nm, which is a typical feature of wide band gap semiconductor metal oxide. The absorption edge may vary with the Ce^{4+}/ Ce^{3+} ratio (Figure 2G). When H_2O_2 was added, the absorption in the range of 280–310 nm and 350–500 nm changed significantly, which could be attributed to two different processes (Figure S8). In order to verify these two independent processes, sodium hydrosulfite

Table 1. Kinetic parameters of catalase-like activity of P – CeO_2 under variable powers of 405 nm and 450 nm laser irradiation

Parameters	Laser Power (mW)	K_m (mM)	v_{max} ($\times 10^{-7}$ M s^{-1})	k_{cat} ($\times 10^{6} s^{-1}$)	k_{cat}/K_m ($\times 10^{8} M^{-1} s^{-1}$)
Dark	0	4.69	11.7	1.22	2.60
405 nm	100	4.58	18.2	1.90	4.15
405 nm	150	4.28	19.1	1.99	4.65
405 nm	200	4.23	21.6	2.26	5.32
450 nm	250	4.86	18.5	1.94	3.99
450 nm	450	4.34	21.3	2.23	5.14
450 nm	650	4.49	21.9	2.29	5.10
450 nm	850	4.04	22.3	2.34	5.79

($Na_2S_2O_4$) was used as a reducing agent to react with P – CeO_2. However, only a decrease in the absorption band at 280–310 nm was observed, and no additional shoulder absorption bands appeared in the 350–500 nm range (Figure 4D). The decrease of the higher energy 280–300 nm absorption band corresponds to the reduction of Ce^{4+} to Ce^{3+},[41] which is consistent with the XPS results showing the decrease of Ce^{4+} content after adding H_2O_2 (Figures 4A and 4B). Therefore, the appearance of new lower energy absorption bands in the visible light region must correspond to a different process. When H_2O_2 was added to the P – CeO_2 solution, the solution quickly changed from colorless to orangish-yellow, and the red shift of the absorption band progressed for 3 min (Figure 4E), similar to the phenomenon observed in previous reports[42] that assigned the red-shift in absorption band to the formation of adsorbed oxygen species.[43] It was unexpectedly found that when the mixed solution was irradiated with laser, the red-shifted absorption band gradually disappeared. When irradiated for 20 min, the absorption band dropped by 2/3, and finally returned to the original P – CeO_2 absorption spectrum with the disappearance of the yellow color (Figure 4F). However, when placed under dark conditions for up to 60 h, the absorption band only dropped by 1/2 (Figure S9). The results showed that the two processes could be greatly accelerated by laser irradiation. Collectively, these results suggested that an intermediate complex from P – CeO_2 and H_2O_2 may form upon mixing of the two.

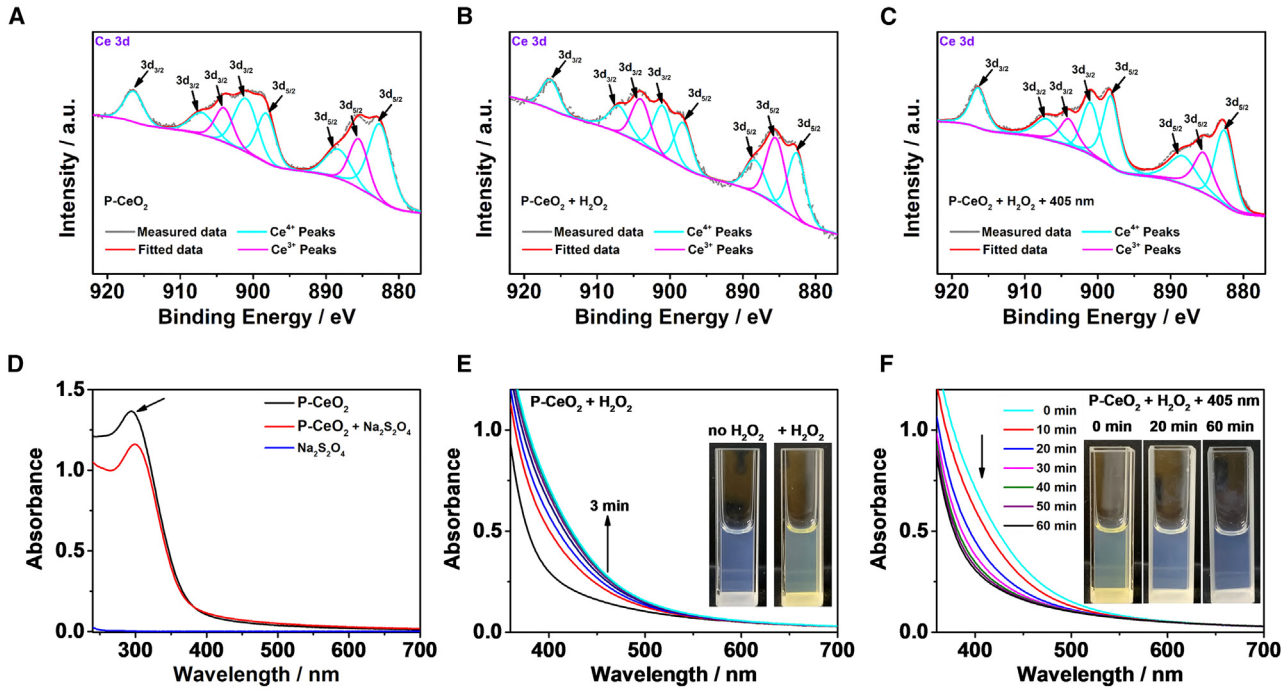

Figure 4. Analysis of surfaces valence states in P-CeO_2 nanozyme

(A–C) High-resolution Ce 3d XPS spectra for (A) P – CeO_2, (B) P – CeO_2 + H_2O_2, and (C) P – CeO_2 + H_2O_2 + 405 nm, respectively.

(D) UV-vis absorption spectra of Na_2S_2O4, P – CeO_2 and P – CeO_2 + $Na_2S_2O_4$.

(E and F) UV-vis absorption changes of P – CeO_2 in 2 mL deionized water with respect to time upon addition of H_2O_2 or H_2O_2 + 405 nm laser irradiation, respectively. The insets are the corresponding sample color changes.

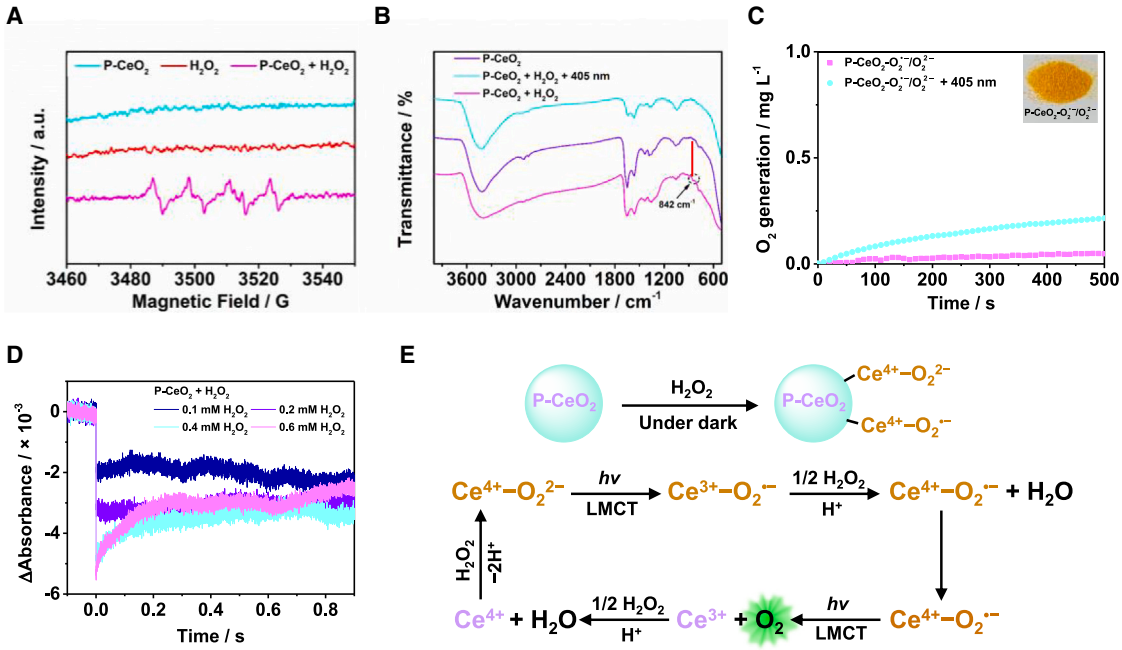

Figure 5. Mechanistic investigation of visible-light-enhanced catalase-mimicking activity of P – CeO_2

(A) ESR spectra of different corresponding situation with the 5,5-dimethyl-1-pyrroline-N-oxide (DMPO) to capture $O_2^{\cdot-}$ free radical.

(B) FT-IR spectra of P – CeO_2, P – $CeO_2 + H_2O_2$, P – $CeO_2 + H_2O_2$ + 405 nm.

(C) O_2 generation of P – CeO_2-$O_2^{\cdot-}/O_2^{2-}$ complexes, P – CeO_2-$O_2^{\cdot-}/O_2^{2-}$ complexes with 405 nm laser irradiation, respectively. The inset shows the P – CeO_2-$O_2^{\cdot-}/O_2^{2-}$ complexes as the orange solid powder.

(D) TA change monitored at 400 nm after pulsed 355 nm excitation of P – CeO_2 in the presence of the indicated concentration of H_2O_2.

(E) Possible reaction mechanism for visible-light-enhanced catalase-mimicking activities of P-CeO_2.

In the above panel of (E), a simplified scheme is presented, omitting a small fraction of Ce^{3+} on the surface of P – CeO_2.

Investigation of the catalytic mechanism

To further explore the reaction mechanism of visible-light-enhanced catalase-mimicking activities. ESR spectroscopy was used to detect radical intermediates. In comparison with P – CeO_2 or H_2O_2 alone, the ESR spectrum of P – $CeO_2 + H_2O_2$ shows a more obvious DMPO – O_2^- – characteristic four peaks with intensity of 1:1:1:1, which indicates the formation of Ce – O_2^- – complex (Figure 5A).[44,45] FT-IR spectroscopy shows that the P – $CeO_2 + H_2O_2$ group has a typical peroxo band at 842nm^{-1}, indicating that Ce – O_2^{2-} complex is also present[41,46] (Figure 5B). However, after laser irradiation, the 842 nm^{-1} peroxo band disappeared. The infrared (IR) band disappearance is consistent with the experimental observation in the aforementioned steady-state UV-vis absorption (Figure 5B and 4F), indicating that the adsorbed oxygen species on the surface of P – CeO_2 can be dissociated by irradiation. To test the dissociated substances, the freshly reacted P – CeO_2 and H_2O_2 mixture was washed by centrifugal precipitation to remove unreacted H_2O_2, and then the dissolved oxygen test was performed. Under laser irradiation, the Ce – O_2^- – / O_2^{2-} complexes can dissociate the adsorbed oxygen species to release O_2 (Figure 5C).

Nanosecond TA spectroscopy was further employed to test the photoinduced electron transfer kinetics for Ce – O_2^- – / O_2^{2-} intermediates (Figure 5D). Indeed, upon pulsed laser excitation into the P – CeO_2 absorption band in the presence of H_2O_2, an absorption bleach at 400 nm where the newly formed Ce – O_2^- – / O_2^{2-} absorbs was observed. The bleach was found instant right after the laser pulse, suggesting the direct excitation of the LMCT band that was lost after Ce^{4+} was reduced to Ce^{3+} by surface absorbed superoxide or peroxide species. Higher H_2O_2 concentrations resulted in larger bleach of the LMCT band, but the bleach will eventually plateau on the sub-second timescale due to the faster charge recombination.

Based on the aforementioned experimental results, a possible reaction mechanism for visible-light-enhanced catalase-mimicking activities of P – CeO_2 is outlined in Figure 5E. Generally, in enzymatic reactions, the substrate binds to the enzyme's active site through specific interactions. The enzyme then catalyzes the conversion of the substrate into a product. Following this, the product is released, allowing the active site to be available for another cycle of substrate binding, catalysis, and product release. The enzymatic reaction is carried out in this cyclic process. Similarly, in the catalytic process of P – CeO_2, catalase-like P – CeO_2 nanozyme decomposes H_2O_2 to produce O_2 and simultaneously Ce^{4+}/ Ce^{3+} redox chemistry occurs. However, O_2 is thermodynamically more favorable to interact with the reduced trivalent cerium and surface oxygen vacancies, so as to form Ce – O_2^- – / O_2^{2-} charge transfer bound species[45,47] resulting in the inability of the product O_2 to be desorbed, and the activity of the reaction site is reduced or

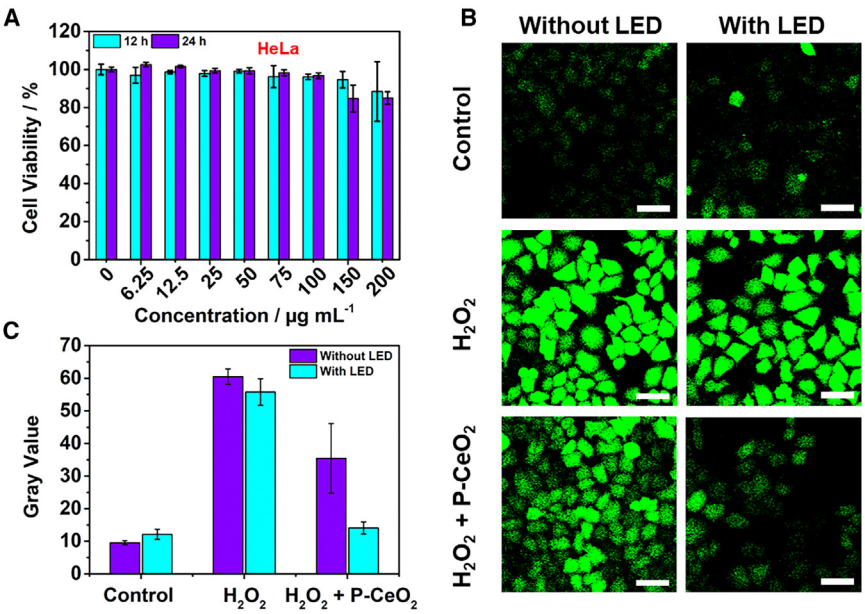

Figure 6. *In vitro* catalytic activity assessment

(A) Cell viability of HeLa cells incubated with different concentrations of P – CeO_2 NPs.

(B) CLSM images of HeLa cells staining by DCFH-DA with different treatments (white light LED, 100 mW cm^{-2}, 5 min).

Scale bar: 50 μm.

(C) The corresponding gray value.

inactivated. But, after laser irradiation, this Ce – $O_2^{\cdot-}$ / O_2^{2-} complex can form free product O_2 through LMCT. At the same time, Ce^{3+} is oxidized by H_2O_2 to Ce^{4+} with active sites, thereby restarting the catalytic cycle of enzymatic reactions, which ultimately leads to visible-light-enhanced catalase-mimicking activities of P – CeO_2 nanozyme.

In vitro catalytic activity assessment

After demonstrating the enhanced catalytic activity under visible light, we further conducted *in vitro* experiments to analyze the use of P – CeO_2 nanozyme as a therapeutic agent for eliminating ROS at the cellular level. The biocompatibility of nanomaterials is crucial for further applications. Therefore, the cytotoxicity of P – CeO_2 was determined in HeLa and normal mouse fibroblast cell line (NIH/3T3) cells using standard cell counting kit-8 (CCK-8) assay. The cell viability of HeLa remained 85.0% (Figure 6A) and NIH/3T3 remained above 98% (Figure S10) even at the high concentration (200 μg mL^{-1}), indicating good biocompatibility of P – CeO_2. Furthermore, intracellular ROS level was monitored by confocal laser scanning microscopy (CLSM) using 2′,7′- dichlorodihydro-fluorescein diacetate (DCFH-DA) probe. Compared with the control group, HeLa cells treated with H_2O_2 showed a strong fluorescence signal (Figure 6B). When P – CeO_2 was added, the ROS fluorescence signal decreased, indicating that the catalase-like activity of P – CeO_2 nanozyme eliminated part of ROS. However, almost all of the green fluorescent signal disappeared in the P – CeO_2 + H_2O_2 + LED group. The results indicated that P – CeO_2 nanozyme possess greater potential to remove ROS from tumor cells under visible light irradiation.

In conclusion, we successfully constructed P – CeO_2 nanozyme with visible-light-enhanced catalase-mimicking activities. The laser intensity and wavelength-dependent enzyme reaction kinetics has been shown to follow the classic Michaelis-Menten mechanism similar to natural enzymes. We discovered that the enhanced catalase-mimicking activities is attributed to the previously unidentified light-induced LMCT, which accelerates the release of O_2 from the Ce – $O_2^{\cdot-}$/O_2^{2-} intermediates in the photocatalytic cycle. Meanwhile, Ce^{3+} is oxidized by H_2O_2 to Ce^{4+} with active sites, thereby closing the catalytic cycle, and finally synergistically leading to enhanced catalytic activity. We believe this work will advance the development of nanozymes with photo-assisted catalytic activities in the photo-biocatalysis field.

Limitations of the study

We successfully constructed P – CeO_2 nanozyme using a simple synthetic procedure with visible-light-enhanced catalase-mimicking activities. Further investigations are warranted to explore the catalase-mimicking activities at elevated temperatures.

RESOURCE AVAILABILITY

Lead contact

Further information and requests for resources could be directed to and will be fulfilled by the lead contact, Ke Hu (khu@fudan.edu.cn).

Materials availability

The authors confirm that the materials are available from the lead contact, Ke Hu (khu@fudan.edu.cn), upon reasonable request.

Data and code availability

All data reported in this paper will be shared by the lead contact upon request.

This paper does not report the original code.

Any additional information required to re-analyze the data reported in this paper is available from the lead contact upon reasonable request.

ACKNOWLEDGMENTS

This study is sponsored by National Key R&D Program of China (2023YFB3507100) and National Natural Science Foundation of China (22173022).

AUTHOR CONTRIBUTIONS

P.L., writing – original draft, methodology, conceptualization. W.Y., review & editing. K.H., review & supervision.

DECLARATION OF INTERESTS

The authors declare no competing interests.

STAR★METHODS

Detailed methods are provided in the online version of this paper and include the following:

- KEY RESOURCES TABLE
- EXPERIMENTAL MODEL AND STUDY PARTICIPANT DETAILS
  - Materials
  - Cell line
- METHOD DETAILS
  - Preperation of $P-CeO_2$ NPs
  - Measurement of O_2 production at different $P-CeO_2$ NPs concentrations
  - O_2 production of $P-CeO_2$ NPs at different pH under light excitation
  - CAT-like activity of $P-CeO_2$ NPs at different pH
  - The preparation of $P-CeO_2-O_2^{\cdot-}/O_2^{2-}$ complexes
  - Detection of $P-CeO_2-O_2^{\cdot-}/O_2^{2-}$ NPs complexes intermediates
  - Characterization
  - The steady-state kinetic assays of P-CeO2 NPs with visible-light-enhanced catalase-mimicking
  - The change of the surface chemical state of $P-CeO_2$ NPs by chemical reduction
  - The investigation of activated surface chemical state of $P-CeO_2$ NPs by photo-redox
  - *In vitro* cytotoxicity
  - Evaluation of anti-oxidant *in vitro*
- QUANTIFICATION AND STATISTICAL ANALYSIS
- ADDITIONAL RESOURCES

SUPPLEMENTAL INFORMATION

Supplemental information can be found online at https://doi.org/10.1016/j.isci.2025.112149.

Received: November 12, 2024
Revised: January 7, 2025
Accepted: February 27, 2025
Published: March 4, 2025

REFERENCES

1. Nandhakumar, P., Kim, G., Park, S., Kim, S., Kim, S., Park, J.K., Lee, N.-S., Yoon, Y.H., and Yang, H. (2020). Metal nanozyme with ester hydrolysis activity in the presence of ammonia-borane and its use in a sensitive immunosensor. Angew. Chem. Int. Ed. Engl. *59*, 22419–22422. https://doi.org/10.1002/anie.202009737.
2. Li, J., Lu, N., Han, S., Li, X., Wang, M., Cai, M., Tang, Z., and Zhang, M. (2021). Construction of bio-nano interfaces on nanozymes for bioanalysis. ACS Appl. Mater. Interfaces *13*, 21040–21050. https://doi.org/10.1021/acsami.1c04241.
3. Gao, F., Shao, T., Yu, Y., Xiong, Y., and Yang, L. (2021). Surface-bound reactive oxygen species generating nanozymes for selective antibacterial action. Nat. Commun. *12*, 745. https://doi.org/10.1038/s41467-021-20965-3.
4. Sun, D., Pang, X., Cheng, Y., Ming, J., Xiang, S., Zhang, C., Lv, P., Chu, C., Chen, X., Liu, G., and Zheng, N. (2020). Ultrasound-switchable nanozyme augments sonodynamic therapy against multidrug-resistant bacterial infection. ACS Nano *14*, 2063–2076. https://doi.org/10.1021/acsnano.9b08667.
5. Zhu, Y., Wang, W., Cheng, J., Qu, Y., Dai, Y., Liu, M., Yu, J., Wang, C., Wang, H., Wang, S., et al. (2021). Stimuli-responsive manganese single-atom nanozyme for tumor therapy via integrated cascade reactions. Angew. Chem. Int. Ed. Engl. *60*, 9480–9488. https://doi.org/10.1002/anie.202017152.
6. Sang, Y., Cao, F., Li, W., Zhang, L., You, Y., Deng, Q., Dong, K., Ren, J., and Qu, X. (2020). Bioinspired construction of a nanozyme-based h2o2 homeostasis disruptor for intensive chemodynamic therapy. J. Am. Chem. Soc. *142*, 5177–5183. https://doi.org/10.1021/jacs.9b12873.
7. Jiang, D., Ni, D., Rosenkrans, Z.T., Huang, P., Yan, X., and Cai, W. (2019). Nanozyme: New horizons for responsive biomedical applications. Chem. Soc. Rev. *48*, 3683–3704. https://doi.org/10.1039/C8CS00718G.
8. Gai, P., Pu, L., Wang, C., Zhu, D., and Li, F. (2023). Ceo2@nc nanozyme with robust dephosphorylation ability of phosphotriester: A simple colorimetric assay for rapid and selective detection of paraoxon. Biosens. Bioelectron. *220*, 114841. https://doi.org/10.1016/j.bios.2022.114841.
9. Chang, J., Yu, L., Hou, T., Hu, R., and Li, F. (2023). Direct and specific detection of glyphosate using a phosphatase-like nanozyme-mediated chemiluminescence strategy. Anal. Chem. *95*, 4479–4485. https://doi.org/10.1021/acs.analchem.2c05198.
10. Gu, C., Zhang, L., Hou, T., Zhu, D., Li, F., and Gai, P. (2024). Unveiling the glucose oxidase-like and catalase-like activities of highly conjugated 3,4,9,10-perylenetetracarboxylic dianhydride for boosting biofuel cells. Adv. Funct. Mater. *34*, 2400617. https://doi.org/10.1002/adfm.202400617.
11. Xiao, G., Li, H., Zhao, Y., Wei, H., Li, J., and Su, H. (2022). Nanoceria-based artificial nanozymes: Review of materials and applications. ACS Appl. Nano Mater. *5*, 14147–14170. https://doi.org/10.1021/acsanm.2c03009.
12. Jiang, P., Zhang, L., Liu, X., Ye, C., Zhu, P., Tan, T., Wang, D., and Wang, Y. (2024). Tuning oxidant and antioxidant activities of ceria by anchoring copper single-site for antibacterial application. Nat. Commun. *15*, 1010. https://doi.org/10.1038/s41467-024-45255-6.
13. Yuan, B., Tan, Z., Guo, Q., Shen, X., Zhao, C., Chen, J.L., and Peng, Y.-K. (2023). Regulating the h2o2 activation pathway on a well-defined CeO2nanozyme allows the entire steering of its specificity between associated enzymatic reactions. ACS Nano *17*, 17383–17393. https://doi.org/10.1021/acsnano.3c05409.
14. Wang, Y., Tan, Z., Zhang, Z., Zhu, P., Tam, S.W., Zhang, Z., Jiang, X., Lin, K., Tian, L., Huang, Z., et al. (2022). Facet-dependent activity of CeO2nanozymes regulate the fate of human neural progenitor cell via redox homeostasis. ACS Appl. Mater. Interfaces *14*, 35423–35433. https://doi.org/10.1021/acsami.2c09304.
15. Lee, S.H., Choi, D.S., Kuk, S.K., and Park, C.B. (2018). Photobiocatalysis: Activating redox enzymes by direct or indirect transfer of photoinduced electrons. Angew. Chem. Int. Ed. Engl. *57*, 7958–7985. https://doi.org/10.1002/anie.201710070.
16. Schmermund, L., Jurkaš, V., Özgen, F.F., Barone, G.D., Büchsenschütz, H.C., Winkler, C.K., Schmidt, S., Kourist, R., and Kroutil, W. (2019). Photo-biocatalysis: Biotransformations in the presence of light. ACS Catal. *9*, 4115–4144. https://doi.org/10.1021/acscatal.9b00656.
17. van Schie, M.M.C.H., Paul, C.E., Arends, I.W.C.E., and Hollmann, F. (2019). Photoenzymatic epoxidation of styrenes. Chem. Commun. *55*, 1790–1792. https://doi.org/10.1039/C8CC08149B.
18. Zhang, J.Z., and Reisner, E. (2019). Advancing photosystem ii photoelectrochemistry for semi-artificial photosynthesis. Nat. Rev. Chem *4*, 6–21. https://doi.org/10.1038/s41570-019-0149-4.
19. Fang, X., Kalathil, S., and Reisner, E. (2020). Semi-biological approaches to solar-to-chemical conversion. Chem. Soc. Rev. *49*, 4926–4952. https://doi.org/10.1039/C9CS00496C.
20. Zhang, S., Zhang, Y., Chen, Y., Yang, D., Li, S., Wu, Y., Sun, Y., Cheng, Y., Shi, J., and Jiang, Z. (2021). Metal hydride-embedded titania coating to coordinate electron transfer and enzyme protection in photo-enzymatic catalysis. ACS Catal. *11*, 476–483. https://doi.org/10.1021/acscatal.0c04462.

21. Tian, Z., Yao, T., Qu, C., Zhang, S., Li, X., and Qu, Y. (2019). Photolyase-like catalytic behavior of CeO2. Nano Lett. *19*, 8270–8277. https://doi.org/10.1021/acs.nanolett.9b03836.

22. Zhang, J., and Liu, J. (2020). Light-activated nanozymes: Catalytic mechanisms and applications. Nanoscale *12*, 2914–2923. https://doi.org/10.1039/C9NR10822J.

23. Sun, M., Xu, L., Qu, A., Zhao, P., Hao, T., Ma, W., Hao, C., Wen, X., Colombari, F.M., de Moura, A.F., et al. (2018). Site-selective photoinduced cleavage and profiling of dna by chiral semiconductor nanoparticles. Nat. Chem. *10*, 821–830. https://doi.org/10.1038/s41557-018-0083-y.

24. Zhang, H., Hao, C., Qu, A., Sun, M., Xu, L., Xu, C., and Kuang, H. (2020). Light-induced chiral iron copper selenide nanoparticles prevent β-amyloidopathy *in vivo*. Angew. Chem. Int. Ed. Engl. *59*, 7131–7138. https://doi.org/10.1002/anie.202002028.

25. Zhang, Y., Villarreal, E., Li, G.G., Wang, W., and Wang, H. (2020). Plasmonic nanozymes: Engineered gold nanoparticles exhibit tunable plasmon-enhanced peroxidase-mimicking activity. J. Phys. Chem. Lett. *11*, 9321–9328. https://doi.org/10.1021/acs.jpclett.0c02640.

26. Liu, R., Cheng, D., Zhou, Q., Niu, F., and Hu, K. (2021). Gold nanoclusters perform enzyme-like photocatalysis for prodrug activation. ACS Appl. Nano Mater. *4*, 990–994. https://doi.org/10.1021/acsanm.1c00014.

27. Kerzig, C., and Wenger, O.S. (2019). Reactivity control of a photocatalytic system by changing the light intensity. Chem. Sci. *10*, 11023–11029. https://doi.org/10.1039/C9SC04584H.

28. Chen, J., Ma, Q., Li, M., Wu, W., Huang, L., Liu, L., Fang, Y., and Dong, S. (2020). Coenzyme-dependent nanozymes playing dual roles in oxidase and reductase mimics with enhanced electron transport. Nanoscale *12*, 23578–23585. https://doi.org/10.1039/D0NR06605B.

29. Huang, Y., Ren, J., and Qu, X. (2019). Nanozymes: Classification, catalytic mechanisms, activity regulation, and applications. Chem. Rev. *119*, 4357–4412. https://doi.org/10.1021/acs.chemrev.8b00672.

30. Wang, H., Wan, K., and Shi, X. (2019). Recent advances in nanozyme research. Adv. Mater. *31*, 1805368. https://doi.org/10.1002/adma.201805368.

31. Montini, T., Melchionna, M., Monai, M., and Fornasiero, P. (2016). Fundamentals and catalytic applications of CeO2-based materials. Chem. Rev. *116*, 5987–6041. https://doi.org/10.1021/acs.chemrev.5b00603.

32. Huang, X., Zhang, K., Peng, B., Wang, G., Muhler, M., and Wang, F. (2021). Ceria-based materials for thermocatalytic and photocatalytic organic synthesis. ACS Catal. *11*, 9618–9678. https://doi.org/10.1021/acscatal.1c02443.

33. Zhang, D.-Y., Liu, H., Li, C., Younis, M.R., Lei, S., Yang, C., Lin, J., Li, Z., and Huang, P. (2020). Ceria nanozymes with preferential renal uptake for acute kidney injury alleviation. ACS Appl. Mater. Interfaces *12*, 56830–56838. https://doi.org/10.1021/acsami.0c17579.

34. Yan, R., Sun, S., Yang, J., Long, W., Wang, J., Mu, X., Li, Q., Hao, W., Zhang, S., Liu, H., et al. (2019). Nanozyme-based bandage with single-atom catalysis for brain trauma. ACS Nano *13*, 11552–11560. https://doi.org/10.1021/acsnano.9b05075.

35. Pirmohamed, T., Dowding, J.M., Singh, S., Wasserman, B., Heckert, E., Karakoti, A.S., King, J.E.S., Seal, S., and Self, W.T. (2010). Nanoceria exhibit redox state-dependent catalase mimetic activity. Chem. Commun. *46*, 2736–2738. https://doi.org/10.1039/B922024K.

36. Yao, C., Wang, W., Wang, P., Zhao, M., Li, X., and Zhang, F. (2018). Near-infrared upconversion mesoporous cerium oxide hollow biophotocatalyst for concurrent ph-/h2o2-responsive o2-evolving synergetic cancer therapy. Adv. Mater. *30*, 1704833. https://doi.org/10.1002/adma.201704833.

37. Liang, X., Xiao, J., Chen, B., and Li, Y. (2010). Catalytically stable and active CeO2mesoporous spheres. Inorg. Chem. *49*, 8188–8190. https://doi.org/10.1021/ic100795p.

38. Sorigué, D., Légeret, B., Cuiné, S., Blangy, S., Moulin, S., Billon, E., Richaud, P., Brugière, S., Couté, Y., Nurizzo, D., et al. (2017). An algal photoenzyme converts fatty acids to hydrocarbons. Science *357*, 903–907. https://doi.org/10.1126/science.aan6349.

39. Sancar, A. (2016). Mechanisms of dna repair by photolyase and excision nuclease (nobel lecture). Angew. Chem. Int. Ed. Engl. *55*, 8502–8527. https://doi.org/10.1002/anie.201601524.

40. Schoefs, B., and Franck, F. (2007). Protochlorophyllide reduction: Mechanisms and evolution. Photochem. Photobiol. *78*, 543–557. https://doi.org/10.1562/0031-8655(2003)0780543PRMAE2.0.CO2.

41. Damatov, D., and Mayer, J.M. (2016). (hydro)peroxide ligands on colloidal cerium oxide nanoparticles. Chem. Commun. *52*, 10281–10284. https://doi.org/10.1039/C6CC03790A.

42. Baldim, V., Bedioui, F., Mignet, N., Margaill, I., and Berret, J.-F. (2018). The enzyme-like catalytic activity of cerium oxide nanoparticles and its dependency on Ce3+surface area concentration. Nanoscale *10*, 6971–6980. https://doi.org/10.1039/C8NR00325D.

43. Wang, Y.-J., Dong, H., Lyu, G.-M., Zhang, H.-Y., Ke, J., Kang, L.-Q., Teng, J.-L., Sun, L.-D., Si, R., Zhang, J., et al. (2015). Engineering the defect state and reducibility of ceria based nanoparticles for improved anti-oxidation performance. Nanoscale *7*, 13981–13990. https://doi.org/10.1039/C5NR02588E.

44. Martínez-Arias, A., Conesa, J.C., and Soria, J. (2007). O2-probe epr as a method for characterization of surface oxygen vacancies in ceria-based catalysts. Res. Chem. Intermed. *33*, 775–791. https://doi.org/10.1163/156856707782169345.

45. Preda, G., Migani, A., Neyman, K.M., Bromley, S.T., Illas, F., and Pacchioni, G. (2011). Formation of superoxide anions on ceria nanoparticles by interaction of molecular oxygen with Ce3+sites. J. Phys. Chem. C *115*, 5817–5822. https://doi.org/10.1021/jp111147y.

46. Li, C., Domen, K., Maruya, K., and Onishi, T. (1989). Dioxygen adsorption on well-outgassed and partially reduced cerium oxide studied by ft-ir. J. Am. Chem. Soc. *111*, 7683–7687. https://doi.org/10.1021/ja00202a003.

47. Sardesai, N.P., Andreescu, D., and Andreescu, S. (2013). Electroanalytical evaluation of antioxidant activity of cerium oxide nanoparticles by nanoparticle collisions at microelectrodes. J. Am. Chem. Soc. *135*, 16770–16773. https://doi.org/10.1021/ja408087s.

STAR★METHODS

KEY RESOURCES TABLE

REAGENT or RESOURCE	SOURCE	IDENTIFIER
Chemicals, peptides, and recombinant proteins		
Cerium(III) nitrate hexahydrate $Ce(NO_3)_3 \cdot 6H_2O$	Admas-beta Co., Ltd.	CAS#10294-41-4
Propanoic acid (C_2H_5COOH)	Admas-beta Co., Ltd.	CAS#79-09-4
Ethylene glycol ($C_2H_6O_2$)	Admas-beta Co., Ltd.	CAS#107-21-1
Sodium hydrosulfite ($Na_2S_2O_4$)	Admas-beta Co., Ltd.	CAS#7775-14-6
Catalase from bovine liver	Admas-beta Co., Ltd.	CAS#9001-05-2
Hydrogen peroxide 30% aqueous solution (H_2O_2)	Sinopharm Chemical Co., Ltd.	CAS#7722-84-1
Ethanol (C_2H_6O)	Sinopharm Chemical Co., Ltd.	CAS#64-17-5
Methanol (CH_3OH)	Shanghai Titan Scientific Co.,Ltd.	CAS#67-56-1
Critical commercial assays		
Cell counting Kit-8	Beyotime Biotechnology Co.,Ltd.	C0037
Dulbecco's Modified Eagle's Medium (DMEM)	ATCC, Sigma-Aldrich and Gibco	11965092
Roswell Park Memorial Institute-1640 (RPMI-1640)	ATCC, Sigma-Aldrich and Gibco	12633020
Fetal bovine serum (FBS)	ATCC, Sigma-Aldrich and Gibco	A5256701
2',7'- dichlorodihydro-fluorescein diacetate (DCFH-DA)	Beijing Solarbio Science & Technology Co., Ltd.	CAS#4091-99-0
Experimental models: Cell lines		
HeLa		N/A
NIH/3T3		N/A
Software and algorithms		
EndNote	EndNote Software	https://endnote.com/downloads/
Origin9	Origin9 Software	https://www.originlab.com/

EXPERIMENTAL MODEL AND STUDY PARTICIPANT DETAILS

Materials

Cerium(III) nitrate hexahydrate ($Ce(NO_3)_3 \cdot 6H_2O$, purity 99.99%), propanoic acid (C_2H_5COOH, purity 99%), ethylene glycol ($C_2H_6O_2$, purity 99%), catalase from bovine liver, and sodium hydrosulfite ($Na_2S_2O_4$, purity 88%) were obtained from Admas-beta Co., Ltd. Hydrogen peroxide 30% aqueous solution (H_2O_2, 30%), ethanol absolute (C_2H_6O, purity 99.7%) were obtained from Sinopharm Chemical Reagent Co., Ltd. Methyl alcohol (CH_3OH, purity 99.5%) was purchased from Shanghai Titan Scientific Co.,Ltd. Cell counting Kit-8 was purchased from Beyotime Biotechnology Co.,Ltd. Dulbecco's Modified Eagle's Medium (DMEM), Roswell Park Memorial Institute-1640 (RPMI-1640), and fetal bovine serum (FBS) were purchased from commercial suppliers (ATCC, Sigma-Aldrich and Gibco). 2′, 7′– dichlorodihydro-fluorescein diacetate (DCFH-DA) were purchased from Beijing Solarbio Science & Technology Co., Ltd. All reagents were purchased from commercial sources and used without further purification.

Cell line

We used HeLa and NIH/3T3 cells from the Chinese Academy of Sciences Shanghai Cell Bank (Shanghai) to study. Cells were incubated at 37°C and 5% CO_2 in DMEM complete medium containing 10% fetal bovine serum.

METHOD DETAILS

Preperation of P − CeO_2 NPs

P − CeO_2 NPs were prepared according to the previous reported with slight modifications.[1] In a typical synthesis, 1.0 g $Ce(NO_3)_3 \cdot 6H_2O$ was dissolved in 1 mL deionized water. Then, 1 mL of C_2H_5COOH and 30 mL of ethylene glycol were added with vigorous stirring to form a homogeneous solution, and the mixture was stirred at room temperature for 30 min. Then, the mixed solution was sealed in an autoclave (50 mL) and heated at 180°C for 200 min. Then the product was washed with water and ethanol three times by centrifugation (13000 rpm for 30 min, 13000 rpm for 20 min, 13000 rpm for 10 min) to remove possible residual ions and

organic solvents in the product. Finally, the precipitate was removed by centrifugation at a speed (2000 rpm/min, 10 min), and the supernatant was retained for other experiments. The sample was dispersed in ethanol solution and its morphology and structure were observed by TEM and HR-TEM.

Measurement of O_2 production at different P − CeO_2 NPs concentrations

The measurement of O_2 production at different P − CeO_2 NPs concentrations was assessed by the dissolved oxygen meter. First, 10 mL tris buffer solution (10 mM pH 7.2) with various P − CeO_2 NPs concentrations (200, 100, 150, 200 μg mL^{-1}) was added to the self-made 20 mL volume reaction device. The reaction flask was sealed using a rubber septum and then flushed with nitrogen gas for 10 min to make the reaction system anaerobic. And add H_2O_2 (working concentration: 10 mM) with a micro-injector, and finally use a dissolved oxygen meter to online test the dissolved oxygen content in the solution at different time points. Unless otherwise specified, all dissolved oxygen was tested in the text need to go through this operation process. The light-enhanced catalase-like activity of various P − CeO_2 NPs concentrations was carried out by adding 405 nm laser (output power: 100 mW) and 450 nm laser (output power: 250 mW) throughout the same measurement process as above.

O_2 production of P − CeO_2 NPs at different pH under light excitation

O_2 production of P − CeO_2 NPs at different pH was assessed by the dissolved oxygen meter. In detail, first, P − CeO_2 NPs solution (working concentration: 200 μg mL^{-1}) was added to 10 mL of 10 mM buffer solution with various pH (3.9, 4.5, 5.5, 6.3), and moved to a self-made reaction device with a volume of 20 mL. The reaction flask was sealed using a rubber septum and then flushed with nitrogen gas for 10 min to make the reaction system anaerobic. And add H_2O_2 (working concentration: 6 mM) with a micro-injector, and finally use a dissolved oxygen meter to online test the dissolved oxygen content in the solution at different time points. The light-enhanced catalase-like activity of P − CeO_2 NPs at different pH was carried out by adding 405 nm laser (output power: 100 mW) and 450 nm laser (output power: 250 mW) throughout the same measurement process as above.

CAT-like activity of P − CeO_2 NPs at different pH

CAT-like activity of P − CeO_2 NPs at different pH was assessed by the dissolved oxygen meter to detect O_2 production. P − CeO_2 NPs solution (working concentration: 200 μg mL^{-1}) was added to 10 mL of 10 mM buffer solution with various pH (3.9, 4.5, 5.5, 6.3, 7.2, 8.6, 9.9, 10.5), and add H_2O_2 (working concentration: 10 mM) with a micro-injector, and finally use a dissolved oxygen meter to online test the dissolved oxygen content in the solution during the 5 min's reaction procedure. At the same time, use a pH meter to test the pH value of the solution before and after the reaction. All experiments were repeated three times.

The preparation of P − CeO_2 − $O_2^{\cdot -}/O_2^{2-}$ complexes

200 μg mL^{-1} of P − CeO_2 NPs was reacted with H_2O_2 (working concentration: 60 mM) for 48 h under dark conditions, then centrifuged and washed three times to remove unreacted H_2O_2, dispersed in pure water, the color of the solution was yellow. The dissolved oxygen content of P − CeO_2 − $O_2^{\cdot -}/O_2^{2-}$ complexes solutions with or without 405 nm laser irradiation (output power: 200 mW) were measured by using the same dissolved oxygen test method as above.

Detection of P − CeO_2 − $O_2^{\cdot -}/O_2^{2-}$ NPs complexes intermediates

5,5-Dimethyl-1-pyrroline-N-oxide (DMPO) spin-trapping adduct was used to detect O_2^{2-}. In brief, the working concentration of the experimental group includes 1) 200 μg mL^{-1} P − CeO_2/100 mM DMPO; 2) 20 mM H_2O_2/100 mM DMPO; 3) 200 μg mL^{-1}P − CeO_2/100 mM DMPO/20 mM H_2O_2; 4) 200 μg mL^{-1} P − CeO_2/20 mM H_2O_2 solution was irradiated by 405 nm laser for 10 min, and then 100 mM DMPO was added. All the sample mixtures were dispersed in 100 μL DMSO solution and reacted for 3 min. The solutions were then displaced into quartz capillaries for ESR test.

Characterization

The morphology and structure of P − CeO_2 NPs was characterized by TEM (HT-7700, Hitachi, Japan). High resolution TEM (HR-TEM) image and energy-dispersive X-ray spectroscopy (EDS) were obtained by Tecnai G2 F20 S-Twin (PEI, USA). The crystal structure of the P − CeO_2 NPs was characterized by powder X-ray diffraction (XRD) (Bruker D2 PHASER, Germany). The UV–vis spectrum was measured by an Agilent Cary 60 spectrometer. The particle size and zeta potential of the nanoparticles were obtained by a Malvern Zetasizer Nano ZS (Malvern Instruments, UK). Confocal fluorescence microscopy images were obtained by a Nikon $C2^+$ confocal fluorescence microscope (Nikon Microsystems, Japan). The surface chemical state and content of the samples were analyzed using X-ray photoelectron spectroscopy (XPS) (PHI 5000C&PHI5300, USA) with Mg K α radiation source. The surface area and pore volume of P − CeO_2 NPs were estimated by ASAP 2020 Plus surface area analyzers. Fourier transform infrared (FT-IR) spectroscopy characterization was carried out on a Nicolet iS10 spectrophotometer (ThermoFisher, USA). The oxygen in the solution was measured by a multifunctional dissolved oxygen analyzer (JPSJ-605F, Leici, China). Electron spin resonance (ESR) spectrometer (Bruker EMXplus) was used to detect $O_2^{\cdot -}$ Fiber optics coupled semiconductor diode lasers with different wavelength for light experiments were obtained by Changchun New Industries.

The steady-state kinetic assays of P-CeO2 NPs with visible-light-enhanced catalase-mimicking

The steady-state kinetic assay was performed at room temperature. For kinetic assay, the experiments were carried out in 10 mL tris buffer solution (10 mM pH 7.2) with containing 200 μg mL^{-1} P $-$ CeO_2 NPs (working concentration), and various concentrations of H_2O_2, and finally use a dissolved oxygen meter to online test the dissolved oxygen content in the solution. The light-enhanced catalase-like activity of P $-$ CeO_2 NPs at different Laser wavelength and power was carried out by adding 405 nm laser (output power: 100 mW, 150 mW, 200 mW) and 450 nm laser (output power: 250 mW, 450 mW, 650 mW, 850 mW) throughout the same measurement process as above. All experiments were repeated three times. The molar concentration of P $-$ CeO_2 NPs was calculated by using the NanoSight NS300 (Malvern Instruments, Malvern, UK) nanoparticle tracking analyzer. The Michaelis-Menten constant was calculated by following equation:

$$\frac{1}{v_0} = \frac{K_m}{v_{max}} \times \frac{1}{[S]} + \frac{1}{v_{max}} \quad \text{(Equation 3)}$$

$$k_{cat} = \frac{v_{max}}{[E]} \quad \text{(Equation 4)}$$

$$\eta = \frac{k_{cat}}{K_m} \quad \text{(Equation 5)}$$

Where v_0 means the initial velocity, K_m represents the Michaelis constant, [S] is the concentration of substrate, and v_{max} is the maximal reaction velocity. k_{cat} represents catalytic number, η describes the catalytic efficiency of an enzyme.

The change of the surface chemical state of P $-$ CeO_2 NPs by chemical reduction

The reduction of P $-$ CeO_2 NPs surface Ce valence was investigated by Cary 60 spectrometer. Sodium dithionite ($Na_2S_2O_4$), as a reducing agent, is often used in the chemical conversion process. We used $Na_2S_2O_4$ as a chemical reducing agent to change the surface valence state of P $-$ CeO_2 NPs. During the experiment, 2 μL of $Na_2S_2O_4$ (0.5 M) was added into 2 mL of P $-$ CeO_2 NPs aqueous solution. The samples were placed in a quartz cuvette, and then the UV-vis absorption spectra before and after the reaction were tested.

The investigation of activated surface chemical state of P $-$ CeO_2 NPs by photo-redox

In order to explore the mechanism of the reaction between H_2O_2 and P $-$ CeO_2 NPs, UV-vis absorption spectra were obtained using Cary 60 spectrometer. During the experiment, 2μL of H_2O_2 (0.5 M) was added into 2μL of P $-$ CeO_2 NPs aqueous solution (200 μg mL^{-1}). Then the UV-vis absorption spectra of the above mixed solution were recorded over time. When the absorption spectrum of the mixed solution no longer changes. The investigation of surface chemical state of P $-$ CeO_2 NPs by photo-redox was carried out by exposing to 405 nm laser irradiation. And recorded its UV-vis absorption spectra over time.

In vitro cytotoxicity

The normal mouse embryonic fibroblast (NIH-3T3) and human cervical cancer (HeLa) cells were purchased from commercial suppliers (ATCC, Sigma-Aldrich and Gibco). The NIH-3T3 and Hela cells were used to assess cell viability. The two cell lines were cultured in the DMEM medium at 37° C in a humidified atmosphere of 5% CO_2. Briefly, the two cell lines were incubated in 96-well plates with 1x 10^4 cells per well for 24 h. The 96-well plate medium was discarded and washed with PBS. Subsequently, complete medium containing P $-$ CeO_2 NPs at a concentration of 6.25, 12.5, 25, 50, 75, 100, 150 and 200 μg mL^{-1} was added to a 96-well plate and then incubated for various time. Cell viability was determined using CCK-8 assay according to a standard protocol.

Evaluation of anti-oxidant *in vitro*

ROS elimination was observed on CLSM. HeLa cells were cultured for 24 h in glass-bottom dishes (35 mm), then incubated with 1 mL of 200 μg mL^{-1} P $-$ CeO_2 NPs for 6 h, followed by incubation with 500 μM H_2O_2 for 30 min. Experiment group were exposed to LED light (100mW cm^{-2}) for 5 min. The old medium was discarded and washed 3 times with PBS. Then, DCFH-DA diluted in 1640 medium without phenol red was added and cultured at 37° C, 5% CO_2 for 30 min. finally, ROS fluorescence signal was detected by CLSM.

QUANTIFICATION AND STATISTICAL ANALYSIS

All data are shown as mean + SD unless otherwise noted. The figures presented in the text were generated using Origin9 from the raw data. Means with standard deviation error bars are presented.

ADDITIONAL RESOURCES

This study has not generated or contributed to a new website/forum or is not part of any clinical trial.